Published in final edited form as:
Neuroimage. 2015 January 15; 105: 198–207. doi:10.1016/j.neuroimage.2014.10.053.

Probing region-specific microstructure of human cortical areas using high angular and spatial resolution diffusion MRI

Manisha Aggarwal[1,*], **David W. Nauen**[2], **Juan C. Troncoso**[2], and **Susumu Mori**[1,3]

[1]Russell H. Morgan Department of Radiology and Radiological Science, Johns Hopkins University School of Medicine, Baltimore, Maryland, USA

[2]Division of Neuropathology, Department of Pathology, Johns Hopkins University School of Medicine, Baltimore, Maryland, USA

[3]F.M. Kirby Research Center for Functional Brain Imaging, Kennedy Krieger Institute, Baltimore, Maryland, USA

Abstract

Regional heterogeneity in cortical cyto- and myeloarchitecture forms the structural basis of mapping of cortical areas in the human brain. In this study, we investigate the potential of diffusion MRI to probe the microstructure of cortical gray matter and its region-specific heterogeneity across cortical areas in the fixed human brain. High angular resolution diffusion imaging (HARDI) data at an isotropic resolution of 92-μm and 30 diffusion-encoding directions were acquired using a 3D diffusion-weighted gradient-and-spin-echo sequence, from the prefrontal (Brodmann area 9), primary motor (area 4), primary somatosensory (area 3b), and primary visual (area 17) cortical specimens (n = 3 each) from three human subjects. Further, the diffusion MR findings in these cortical areas were compared with histological silver impregnation of the same specimens, in order to investigate the underlying architectonic features that constitute the microstructural basis of diffusion-driven contrasts in cortical gray matter. Our data reveal distinct and region-specific diffusion MR contrasts across the studied areas, allowing delineation of intracortical bands of tangential fibers in specific layers layer I, layer VI, and the inner and outer bands of Baillarger. The findings of this work demonstrate unique sensitivity of diffusion MRI to differentiate region-specific cortical microstructure in the human brain, and will be useful for myeloarchitectonic mapping of cortical areas as well as to achieve an understanding of the basis of diffusion NMR contrasts in cortical gray matter.

Keywords

cortical areas; diffusion MRI; human; gray matter; microstructure

[*]Address correspondence to: Manisha Aggarwal, Ph.D., 334 Traylor Building, Johns Hopkins University School of Medicine, 720 Rutland Avenue, Baltimore, MD 21205, USA, maggarw2@jhu.edu, Phone: (410) 955-9483, Fax: (410) 614-1948.

INTRODUCTION

Diffusion MRI (dMRI) utilizes water molecular diffusion as an endogenous probe of tissue microstructure. Based on detecting the Brownian motion of water molecules undergoing restricted diffusion, dMRI provides a powerful contrast mechanism to investigate the structural organization of nervous tissue. Techniques including diffusion tensor imaging (Basser et al., 1994), high angular resolution diffusion imaging (HARDI) (Tuch et al., 2002), and diffusion spectrum imaging (Wedeen et al., 2005), have been developed to infer tissue microstructural properties from the diffusion-driven NMR signal decay. While the efficacy of these techniques for characterization of white matter tracts in the brain is well established, the potential of diffusion-based MRI to resolve the microstructure of gray matter remains relatively less exploited. Diffusion in gray matter regions, such as the cerebral cortex, encounters less coherently organized tissue microenvironments. Relative contributions to diffusion restriction in the gray matter arise from multiple microscopic barriers (including cell somata, axons, and dendritic arbors) with varying structural orientations, resulting in increased complexity and higher isotropy of diffusion in these regions.

The cortical gray matter in the human brain has a heterogeneous layered architecture. Specific areas of the cerebral cortex exhibit distinct cyto- and myelo-architecture, which are thought to relate to their functional differentiation and underlying complexity of neural processing (Zilles and Amunts, 2012). The region-specific heterogeneity of this layered architecture forms the structural basis of mapping of cortical areas (Amunts et al., 2002; Brodmann, 1909; Geyer et al., 2011), and has been widely investigated using histologic sectioning and in-plane immunostaining techniques. Myeloarchitecture of cortical areas mapped using techniques such as silver impregnation and Weigert staining shows distinct radial and tangential fibers across specific layers (Nieuwenhuys, 2013; Vogt and Vogt, 1919). For instance, tangentially-oriented fibers in the cerebral cortex constitute the horizontal plexus of dendritic and axonal projections in cortical layer I and the internal and external bands of Baillarger (Baillarger, 1840), of which the external band is the most prominent in parts of the primary visual cortex. Three-dimensional (3D) characterization of cortical gray matter using diffusion-based MRI can potentially afford additional insights into the complex regional microstructure and layer-specific connectivity compared to in-plane histological methods, but remains technically challenging.

Recent studies over the last decade have examined diffusion MR contrasts in the cerebral cortex. In the developing cortex, high anisotropy of diffusion is well established in both humans and animal models (Aggarwal et al., 2014; Kroenke et al., 2007; McKinstry et al., 2002), and reflects the structural organization of the transient radial glial scaffolding. In comparison, the adult cerebral cortex is characterized by significantly reduced diffusion anisotropy. There are relatively few reports on dMRI of the adult human cortex, that have found primarily radial orientation of diffusion in cortical gray matter, both in vivo (Heidemann et al., 2010; Jaermann et al., 2008; Truong et al., 2014) and in fixed brains (McNab et al., 2009; Miller et al., 2011). There is also reported evidence of diffusion tangential to the cortical surface in parts of the somatosensory cortex (Anwander et al., 2010; McNab et al., 2013). Based on observed diffusion orientations in the ex vivo pig brain, Dyrby et al. reported the delineation of two parallel inner and outer rims in the

cortical gray matter (Dyrby et al., 2011). More recently, HARDI of human visual cortex specimens at resolutions of 242–300 μm was shown to delineate multiple components in orientation density functions in the stria of Gennari and deeper cortical layers (Kleinnijenhuis et al., 2013; Leuze et al., 2014), allowing reconstruction of tangential fibers in the primary visual area (Leuze et al., 2014).

Current efforts on structural parcellation of cortical areas in the human brain using MRI are largely based on analyzing white matter connectivity and cortical folding patterns, both in vivo (Anwander et al., 2007; Behrens and Johansen-Berg, 2005) and ex vivo (Augustinack et al., 2014; Fischl, 2013). Mapping the microstructure of cortical gray matter and investigating its regional architectonic differentiation using dMRI, however, is technically hindered by both the intrinsically low anisotropy of diffusion in gray matter microenvironments and the tradeoff in the diffusion-weighted signal-to-noise ratio introduced with the increasing level of spatial resolution necessary to resolve the laminar architecture across cortical depth. Given that the cortical thickness in the human brain ranges from 1 to 4.5 mm across cortical areas (Fischl and Dale, 2000), high resolution acquisition for dMRI is crucial for minimization of partial volume effects in order to investigate diffusion contrasts specific to cortical layers. In addition, further advances in the investigation of cortical structure and its architectonic differentiation using dMRI are also dependent on our understanding of the microstructural correlates of diffusion-driven contrasts in cortical gray matter, and the architectural features that contribute to the observed anisotropy of diffusion, which remain largely unclear. Ex vivo studies of cortical areas, which enable direct and *in situ* comparison of diffusion-weighted contrasts with histological staining in the same subjects, can potentially yield important insights into deciphering the microstructural basis of diffusion contrasts in the human cortex.

In this study, we investigate the potential of diffusion MRI to probe the microstructure of cortical gray matter and its region-specific heterogeneity across cortical areas in the fixed human brain. Combined high angular and spatial resolution achieved by means of a diffusion-weighted gradient- and spin-echo sequence with twin-echo navigation was used to acquire 3D diffusion micro-imaging data from the prefrontal, visual, primary motor, and primary somatosensory cortical areas from three human brains. Furthermore, the dMRI findings in different cortical areas were compared with subsequent histological silver impregnation of the same specimens, in order to elucidate the underlying region-specific architectonic features that constitute the structural basis of diffusion-driven contrasts in cortical gray matter.

MATERIALS AND METHODS

Cortical specimens and preparation

Study specimens from the prefrontal, primary motor, primary somatosensory, and visual cortices (n=3 each) were obtained from three adult human cadaver brains (male, age 37–74 years), provided by the Brain Resource Center at the Johns Hopkins University School of Medicine under Institutional Review Board approved protocols. The brains were fixed in 10% neutral buffered formaldehyde for more than two months, with post-mortem fixation intervals of < 24 h. Tissue blocks (approximately 15 × 15 × 22 mm^3) were dissected from

the left hemisphere of each brain, from the prefrontal cortex in the superior frontal gyrus (Brodmann area 9), primary motor cortex in the caudal wall of the precentral gyrus (Brodmann area 4), primary somatosensory cortex in the rostral wall of the postcentral gyrus (Brodmann area 3b), and the visual cortex around the calcarine sulcus (Brodmann area 17). The blocks were cut orthogonal to the cortical surface and included part of the subjacent white matter. 72 h prior to imaging, specimens were transferred to phosphate buffered saline at 4°C with 2 mM gadopentetate dimeglumine (Gd-DTPA, Berlex Imaging, Wayne, NJ, USA) for T_1 shortening and to wash out the fixative. For MRI, the specimens were inserted in 15-mm NMR tubes which were filled with Fomblin® (Solvay Solexis, Thorofare, NJ, USA) for susceptibility matching and to prevent dehydration. The tubes were placed in a vacuum chamber for 10 min prior to MR experiments for expulsion of any air bubbles trapped in interstices of the sulci.

HARDI acquisition

Diffusion MR experiments were performed on a vertical-bore 11.7 T NMR spectrometer (Bruker Biospin, Billerica, MA, USA), equipped with a Micro2.5 imaging probe with actively shielded triple-axis gradients capable of generating 120 G/cm. A birdcage volume coil with 15-mm inner diameter was used for RF transmission and signal reception. During imaging, the temperature of the specimens was maintained at 37°C via thermostatically controlled airflow. HARDI data of cortical specimens were acquired using a 3D diffusion-weighted gradient and spin echo (DW-GRASE) sequence (Aggarwal et al., 2010), with 4 refocusing pulses per excitation and acquisition of three echoes after each refocusing pulse. The acquisition parameters were: echo time (TE) = 35 ms, repetition time (TR) = 600 ms, two signal averages, and receiver bandwidth of 90 kHz. Non-phase-encoded twin-navigator echoes (Mori and van Zijl, 1998) at the end of each readout echo train were acquired to map and correct for phase modulation of the *k*-space data along both phase-encode axes due to eddy current (along k_y) and off-resonance (along k_z) effects. Two minimally diffusion-weighted (b0) images and 30 images in uniformly distributed diffusion-encoding directions (Jones et al., 1999) were acquired (b-value=2000 s/mm^2), using bipolar diffusion-weighting gradients with double refocusing (Reese et al., 2003) and gradient duration (δ)/separation (Δ) = 3.2/14 ms. The acquisition time was ~28 h for HARDI at a resolution of 92 × 92 × 92 μm^3 with fully-sampled *k*-space. The *k*-space data were zero-filled by a factor of two prior to Fourier transformation. For the visual cortex specimens, co-registered T_2-weighted images were additionally acquired for anatomical reference, using a 3D rapid acquisition with relaxation enhancement (RARE) sequence with the following parameters: rare-factor of 8, effective TE/TR = 42/800 ms, and 4 signal averages. Signal-to-noise ratios (SNR) were calculated as S/σ, where S was the mean signal intensity within a region of interest defined within the cortical gray matter in b0 images, and σ the standard deviation of the background noise.

Data analysis

Images were reconstructed using IDL (ITT Visual Information Solutions, Boulder, CO, USA). From the diffusion-weighted images, parametric maps of fractional anisotropy (FA) and direction-encoded color (DEC) maps were first calculated by fitting the DW signal intensity profiles to the tensor model using log-linear fitting (Jiang et al., 2006). The HARDI

data were processed using MRtrix (Tournier et al., 2012) with constrained spherical deconvolution (CSD) to model multiple fiber orientations within each voxel (Tournier et al., 2007). The spherical harmonic coefficients for the response function were estimated from a mask of high anisotropy voxels defined in the subcortical white matter of each specimen, which served as a reference region containing single-fiber voxels. Fiber orientation distribution functions (fODFs) were reconstructed using CSD with a maximum spherical harmonic order (l_{max}) of 6 for 30 diffusion directions. For visualization, track-density imaging (TDI) maps (Calamante et al., 2010) of cortical areas were generated using fODF-based probabilistic streamline tracking (Behrens et al., 2003). The parameters used for tracking were: step size of 8 μm, maximum angle between steps = 45°, minimum track length = 0.5 mm, and a termination criterion of CSD fiber-orientation distribution amplitude < 0.08. A 10-μm grid size was used to generate TDI maps.

For quantitative analyses of cortical anisotropy, FA profiles across cortical depth were extracted perpendicularly to a central line between layer I/pial boundary and layer VI/white matter interface. The boundary between gray matter and white matter was defined using intensity-based segmentation of b0 images in RoiEditor (www.mristudio.org). The centerline between the outer (between layer I and pial boundary) and inner (between layer VI and white matter) cortical contours was calculated based on a skeletonization algorithm using Matlab (Mathworks Inc., Natick, MA, USA), and FA values were measured along profiles normal to the centerline that extended from the outer to the inner contour. Individual profiles were normalized to a cortical depth of 100% measured from the pial surface, to correct for regional and inter-subject variation in absolute cortical thickness (Eickhoff et al., 2005). Averaged FA profiles for each specimen were obtained by taking the mean of FA values along cortical depth profiles contained within regions-of-interest of 4–5 mm thickness, which were selected within relatively flat areas in the cortical gray matter. Statistical comparisons of FA measurements were done using Wilcoxon rank-sum tests, as the FA values were not normally distributed. All statistical tests were performed using Matlab.

Histological processing

Following MRI, the same tissue specimens were processed for histological analysis to compare diffusion MR contrasts with myeloarchitecture of the studied cortical areas. The specimens were embedded in paraffin blocks, and sectioned into 40-μm thick sections. Silver impregnation histology was performed on select slides using Hirano's modification of the Bielschowsky silver staining method for labeling axons and neuronal processes (Yamamoto and Hirano, 1986). Briefly, deparaffinized sections were impregnated in 20% silver nitrate solution for 30 min. The slides were then washed thoroughly with distilled water and immersed in 20% silver nitrate solution titrated with concentrated ammonium hydroxide. After 15 min, the slides were washed in ammonia water and developed individually in the developer (100 ml of distilled water, 20 ml of formaldehyde, 3 drops of concentrated nitric acid, and 0.5 g of citric acid) added to titrated silver nitrate solution, for 3–5 min until fully developed. Slides were then rinsed in warm water, fixed in 5% sodium thiosulfate solution, and dehydrated through 95% alcohol and xylene. Images were captured

under a Zeiss AxioObserver.Z1 microscope (Carl Zeiss Microscopy, Thornwood, NY, USA) equipped with an AxioCam MRc camera, with a 4x objective.

RESULTS

The mean SNR in b0 images measured in regions-of-interest within the cortical gray matter was 62.8 ± 10.1. Fig. 1 shows DEC maps of area 9 in the prefrontal cortex, which revealed a primary orientation of diffusion radial to the cortical surface, with two intervening zones marked by tangential anisotropy (white arrows in Fig. 1A) that were resolved running parallel to the cortical surface. The outermost cortical layer (layer I) was clearly demarcated in DEC contrasts, by a sharp transition from the radially-oriented anisotropy of underlying layers at the layer II/I interface (asterisk in Fig. 1C). Quantitative FA measurements plotted as a function of cortical depth in the three subjects (Fig. 1B) indicated a distinct laminar profile across the gray matter of area 9. Two separate local minima of significantly ($p<0.002$) low FA compared to adjacent layers were evident across the cortical depth, with two additional local minima resolved adjacent to the gray-white matter boundary in layer VI, and in the superficial layer I. Comparison with silver impregnation of area 9 (Fig. 1D) revealed prominent vertically-oriented fascicles extending from the subcortical white matter, with a dense plexus of faintly-labeled horizontal fibers constituting the inner band of Baillarger (ibB) and relatively diffuse horizontal fibers in the outer band of Baillarger (obB). Tangential fibers were also evident adjacent to the gray-white matter boundary in layer VI (Fig. 1D). fODFs in cortical laminae reconstructed from the HARDI data are shown in Fig. 1C. In the inner zone of low FA corresponding to the ibB, estimated fODFs indicated two prominent orientations with radial and tangential peaks, which reflected the microstructural organization of radial and orthogonally-crossing horizontal fibers evident in the ibB in silver-impregnated sections (black arrow in Fig. 1D). In contrast, layers adjoining the ibB exhibited dominant radial fODF peaks with less pronounced secondary peaks (Fig. 1C), which were observed to be coincident with the predominant vertical orientation of stained fascicles evident in the infragranular layers of area 9 (Fig. 1D).

Diffusion microimaging contrasts in the pre- and postcentral gyri, containing the primary motor (M1, area 4) and primary somatosensory (S1, area 3b) cortices, are shown in Fig. 2. In comparison to area 9, area 4 was marked by an absence of conspicuous horizontal inner and outer bands of Baillarger. Further, FA and DEC maps revealed markedly different diffusion contrasts between the M1 and S1 areas. In area 4, we found diffusion anisotropy oriented primarily radial to the pial surface across the width of the gray matter up to the layer II/I border. Notably, the M1 cortex was marked by a narrow intermediate zone that exhibited significantly ($p<0.001$) higher FA compared to inner and outer adjacent gray matter regions and was delineated coursing parallel to the cortical surface in area 4 of all three subjects (Fig. 2A). In comparison, in area 3b, an internal band of low FA was observed corresponding to 69.2 ± 4.1 % of cortical depth, while relatively strong radial anisotropy was evident along the rest of the cortical thickness up to the layer II/I interface (Fig. 2B). The distinct diffusion patterns resolved in the M1 and S1 areas can be clearly seen in the quantitative FA profiles across cortical depth in Fig. 2C. In addition, the boundary between subcortical white matter and cortical layer VI was less distinct in area 4 in both b0 and

diffusion-weighted contrasts, whereas a sharp transition from the white matter to cortical gray matter could be demarcated in area 3b (Fig. 2A-B).

The region-specific differences in cortical microstructure resolved between areas 4 and 3b are further seen with the estimated fiber orientation distributions across cortical depth and comparison with silver-impregnation in Fig. 3. In area 4, estimated fODFs exhibited radial and tangential components in proximity to the gray-white matter interface, reflecting an indistinct transition from the subcortical white matter to layer VI (panel *c* in Fig. 3A). This was also evidenced by densely-labeled radial and tangential fibers at the gray-white matter border in silver-impregnated sections (Fig. 3A). In the intermediate zone of higher FA (corresponding to the peak in FA profiles in Fig. 2C), we found dominant radial peak orientations in the reconstructed fODFs (panel *b* in Fig. 3A). Radial components of fODFs were also apparent in parts of the adjoining outer laminae, however the estimated fODFs across this region were less well-resolved, indicating a higher uncertainty in the determination of diffusion orientation (panel *a* in Fig. 3A). Histological sections revealed a high density of vertically-oriented fibers and apical dendrites of layer V pyramidal neurons in the mid-cortical layers (III-V) of area 4. In comparison, the adjoining outer region (layer II) was faintly stained and marked by an absence of conspicuous fibers in silver-stained sections (Fig. 3A). In area 3b, dominant radial fODF peaks were resolved in outer cortical laminae, while the internal band of low FA exhibited less coherently organized structure evidenced by dispersed fODF peak orientations (Fig. 3B). Silver-impregnation of the same region highlighted a large number of tangential fibers in the infragranular layers, along with fine vertically-oriented fibers seen extending to layer III (Fig. 3B).

Fig. 4 shows the laminar architecture of the visual cortex (Brodmann area 17) resolved with dMRI. A prominent feature in the primary visual area (V1) is the band of tangential myelinated fibers in layer IVb or the stria of Gennari (soG), which appears as a hypointense band in b0 and T_2w images (Fig. 4A). The DEC maps showed striking contrasts to delineate the tangential orientation of fibers in the soG coursing parallel to the cortical surface in area 17 (white arrow in Fig. 4A). In addition, a second narrower band of tangential fibers was resolved in parts of area 17 in DEC contrasts (white arrowhead in Fig. 4A). This inner band corresponded to the ibB in cortical layer V, and was most prominently delineated in cortical tissue examined adjacent to the occipital pole (Fig. 4A). Two additional bands marked by tangential anisotropy were delineated at the pial surface and the gray-white matter boundary, in layers I and VI, respectively. The distinctly striated appearance of area 17 resolved on the basis of layer-specific diffusion orientations is clearly seen in DEC maps in Fig. 4. A sharp structural transition from area 17 to the extrastriate secondary visual area V2 (Brodmann area 18) could be demarcated in DEC contrasts, based on the absence of prominent tangential bands in area 18 (indicated by the dashed lines in Fig. 4A). Comparison with silver staining revealed that the change in DEC contrasts at the V1-V2 interface (white arrowhead in Fig. 4B) mirrored the transition in the laminar structure and layer-specific myeloarchitecture seen with silver-impregnated sections captured at the level of the V1-V2 border (Fig. 4B). In contrast to the striate area 17, the DEC maps showed radially-oriented anisotropy across cortical depth in a region adjoining the V1-V2 border, and a single

intervening zone of tangential diffusion corresponding to the ibB (asterisk in Fig. 4A) could be delineated in area 18.

Quantitative FA measurements across cortical depth showed markedly different profiles for areas 17 and 18 (Fig. 4C). Corresponding T_2w intensity profiles are also plotted in Fig. 4C for comparison. Compared to the hypointense band delineated in T_2w contrasts, a more distinct laminar structure was evidenced by the FA curves across cortical depth, with separate local minima corresponding to bands of crossing tangential fibers resolved in specific cortical layers (Fig. 4C). Further, as seen in the plots in Fig. 4C, the minimum in the b0 and T_2w intensity profiles of area 17 showed a partial overlap, but did not coincide precisely, with the local minimum in the FA profile corresponding to the band of tangential fibers in the soG. Compared to the minimum resolved in the FA profile, the region of hypointensity in T_2w and b0 profile curves exhibited a shift along the cortical depth (Fig. 4C). This observation was consistent across all three visual cortex specimens examined (supplementary Fig. S1). Note that the plot in Fig. 4C shows the profile for area 17 in the region adjacent to the V1-V2 boundary, where the ibB can be most clearly delineated. FA and DEC maps showing demarcation of the soG in orthogonal planes through the visual cortex and the fiber orientation distributions reconstructed from CSD are shown in Fig. 5. Estimated fODFs in area 17 revealed strong tangential components in the horizontal band corresponding to the soG, compared to adjoining inner and outer cortical layers (Fig. 5C). TDI maps generated from fODF-based probabilistic tracking indicated a band of dense tangential fibers (~300 μm thick) interweaving through radially-oriented processes in the soG (Fig. 5E), which corresponded to the arrangement of crossing radial and horizontal fibers seen with Bielchowsky silver staining of area 17 at the level of the soG (Fig. 5D).

Fig. 6 compares the regional fiber architecture in the astriate M1 cortex (area 4) and the bistriate V1 cortex (area 17) reconstructed from the dMRI data, along with silver-impregnated sections of the two areas. TDI maps of area 4 indicated radial processes extending from the subcortical white matter and dispersed tangential fibers in infragranular layers (V-VI), with the absence of distinct coherent tangential bands of fibers corresponding to the ibB and obB (Fig. 6A). These observations were consistent with the myeloarchitecture of area 4 seen with silver impregnation (Fig. 6A). In area 17, a tangentially-oriented band of intracortical fibers in layer IVb and a relatively less well-defined band of fibers in layer V were resolved coursing orthogonally through radially-oriented fibers, which corresponded to the arrangement of labeled axonal fibers and neurites evident in silver-stained sections (white arrows in Fig. 6B). In both area 4 and area 17, the superficial molecular layer (layer I), which consists of horizontal nerve fibers that synapse with dendritic arbors of pyramidal cells, was clearly delineated (asterisks in Fig. 6A-B). In layer I, fibers ran tangentially along the cortical surface both parallel and perpendicular to the plane of the radial and horizontal fibers seen in underlying layers. The extent of this superficial layer corresponded to the densely stained outer layer I seen with Bielschowsky silver-staining, but the orientations of both in-plane and through-plane fibers in this layer were difficult to resolve with corresponding histological sections in a single plane (Fig. 6A–B).

DISCUSSION

This study demonstrated the microstructure of human cortical gray matter and its regional differentiation across cortical areas revealed with high resolution diffusion MRI. Using 3D DW-GRASE based acquisition, which offers a 12-fold acceleration factor compared to spin-echo sequences, combined high spatial and angular resolution could be achieved for dMRI, which revealed distinct and region-specific diffusion contrasts in the prefrontal, primary motor, primary somatosensory, and visual cortical areas. We found that anisotropy profiles across cortical depth exhibit region-specific diffusion signatures for Brodmann areas 9, 4, 3b, 17, and 18. Furthermore, the dMRI contrasts corresponded closely to the region-specific laminar structure and myeloarchitecture of the studied cortical areas, as evidenced by comparison with histological silver-impregnation. Together, these findings indicate unique sensitivity of diffusion MRI to probe the microstructure of cortical gray matter and characterize its regional laminar differentiation across cortical areas in the human brain.

Diffusion MR-based characterization of cortical heterogeneity has been examined in recent studies. Predominantly radial diffusion in the primary motor cortex with tangential diffusion observed in parts of the somatosensory cortex was reported in previous studies, in vivo and ex vivo (Anwander et al., 2010; McNab et al., 2013). Cortical depth-dependence of diffusion anisotropy has been shown in an in vivo DTI study at 3T (Truong et al., 2014). With higher resolution dMRI of visual cortex specimens, Leuze et al. (2014) delineated four laminae in the primary visual area based on observed diffusion orientations. Other studies have reported the use of features extracted from CSD analysis of HARDI profiles to discriminate cortical regions in the human brain (Haroon et al., 2010; Nagy et al., 2013).

In our study, diffusion contrasts clearly differentiated the astriate (area 4), unistriate (area 18, with only the ibB evident), and bistriate (areas 17, 9) cortical areas based on their region-specific laminar myeloarchitecture. While stripes of Baillarger in the V1 cortex are heavily myelinated, our data also revealed sensitivity of diffusion-driven contrasts to the weakly-stained plexus of horizontal fibers in the prefrontal area 9, evident in both the DEC maps and the resolved fiber orientation distributions across this region (Fig. 1). Radial diffusion anisotropy was observed in the intrastriate layer between the bands of Baillarger and in outer cortical layers (II, III), attributed to axons from the subcortical white matter and dendritic processes that ascend across the cortical depth to upper layers (III, II, and I). In the substriate area, strong radial and tangential diffusion components were resolved in most areas, which reflected the underlying myeloarchitecture of layer VI adjacent to the gray-white matter transition. Reconstruction of track density maps from the HARDI data showed close correspondence to region-specific cortical microstructure demonstrated by silver staining (Fig. 6), which is largely specific to the cytoskeletal components of axons and dendrites. Further, the molecular layer (I) was clearly delimited in dMRI contrasts across all cortical regions examined.

Data shown in Figs. 2–3 demonstrated distinct diffusion profiles across the cortical gray matter in the walls of the pre- and postcentral gyri, with overall cortical depth-dependent characteristics that were reproducible across samples from the three subjects. These findings suggest that areas 4 and 3b can be distinguishable on the basis of their specific diffusion MR

signatures. The indistinct transition from the white matter to layer VI in the M1 cortex versus the S1 cortex observed with dMRI is also consistent with previous cytoarchitectonic studies comparing the pre- and postcentral gyri (Zilles and Amunts, 2012). A tripartite laminar appearance of area 4 in double inversion recovery-based T1 contrasts was reported in a previous study (Kim et al., 2009). In our work, comparison with silver impregnation revealed a high density of vertically-oriented fibers and pyramidal apical dendrites in the midcortical layers of area 4 (Fig. 3A), which contributed to the intermediate zone of higher radial anisotropy observed in the dMRI data (FA, DEC maps in Figs. 2A and 3A). Our findings in Figs. 2–3 also suggest that additional architectonic features potentially contribute to the diffusion-driven contrast. For instance, radial anisotropy was observed in the cell-dense and myelin-sparse upper cortical layers, more prominently in area 3b. These layers did not exhibit conspicuously labeled fibers in silver-stained sections. It is known that cells in cortical layers exhibit a columnar arrangement, and apical dendrites that extend across the upper cortical layers to the outermost layer I can be clearly visualized with specific histologic stains, e.g. MAP2 (Preuss and Coleman, 2002). Compared to area 4, area 3b is also characterized by a higher cell packing density in the supragranular layers (White et al., 1997). Further comparisons with more specific histologic stains may therefore be needed to decipher the relative contributions from these architectonic features to the diffusion-driven contrasts in this region.

In the visual cortex, our data demonstrated layer-specificity of diffusion MR contrasts as seen in Figs. 4 and 5. In particular, the sharp structural transition between area 17 and area 18 resolved with the dMRI data mirrored the underlying shift in the layered architecture across the V1-V2 border demonstrated by silver impregnation (Fig. 4B). Further, our findings in the visual cortex also reflect the distinctive myeloarchitecture of this transition region seen in previous histological studies. The border between areas 17 and 18 is known to have two small subareas, a region with the appearance of the ibB on one side (in area 17) and a region with densely packed radial fibers on the other (in area 18), that have been examined previously in histological sections through this region (Zilles and Amunts, 2012). Data in Figs. 4–5 indicate that this structural transition and its myelo-architectonically distinct subregions between the V1 and V2 areas could be delineated in diffusion-based contrasts, and more importantly, allow the layered architecture across this region to be three-dimensionally examined and studied in arbitrary planes of sectioning across the gray matter in the same cortical specimen (FA, DEC maps in Figs. 4–5). This can be particularly useful given the relatively high inter-subject variability in visual cortex areal borders in the folds of the occipital lobe (Amunts et al., 2000). Additionally, the dMRI contrasts clearly differentiated the outer cortical layer (layer I, indicated in Fig. 1 and Fig. 6), a cell-sparse layer which consists of dispersed dendritic arbors and intracortical axonal fibers running mostly tangential to the cortical surface. As seen in Fig. 6, axonal and dendritic fibers in layer I often run perpendicular to the plane of both the radially-oriented neurites and the tangential axons in the bands of Baillarger, and are therefore difficult to examine with histological sections through the cortex in a given plane.

In this study, the minimum in b0 and T_2w signal intensities in the visual cortex did not coincide precisely with the band of tangential fibers in layer IV delineated with dMR contrasts (the plot in Fig. 4C). A similar observation was reported in a previous dMRI study

by Kleinnijenhuis et al. (2013), that showed a shift in the FA minimum towards the pial surface relative to the minimum in multiple gradient echo intensity profiles in the visual cortex. Consistent with their report, the minimum in mean diffusivity in our data coincided with the hypointense band in T_2w profiles (data not shown), while the local FA minimum showed a partial shift towards the pial surface that was consistent across all subjects. T_2w tissue contrasts are influenced by physiological factors that include myelin density, proton density, and iron content, all of which are known to show variation in laminar distribution across the gray matter of the visual cortex (Barbier et al., 2002; Fukunaga et al., 2010). Both myelin and iron content are more abundant in inner cortical layers compared to outer layers, which would explain the overall shape of the T_2w intensity curves in Fig. 4c. Our data indicate that the local FA minimum corresponds to the band of crossing tangential and radial fibers in layer IVb, as evidenced by the DEC maps and the strong tangential components in the estimated fODFs. It is probable that the mesh-like microstructure of the outer adjoining layer IVa, ~250 μm thick (Preuss and Coleman, 2002), could contribute in part to the lower anisotropy region in the dMRI data. However, based on current observations, our knowledge of potential contributions of architectonic features to the observed cortical depth mismatch between T_2w and diffusion contrasts is incomplete. Further investigation with parametric (T_2/T_2^*) maps and compartment models of diffusion (Zhang et al., 2012) with specific immunohistochemical stains could help tease out the microstructural correlates and underlying contrast mechanisms that contribute to the observed shift between T_2w and diffusion-driven contrasts in the soG.

Finally, the dMRI data in our study were acquired on a single shell with a *b*-value of 2000 s/mm^2 in 30 diffusion directions. The increasing complexity of gray matter microstructure in the human cortex seen in our data also lends itself to advanced multi-compartment models of diffusion, including neurite density and orientation dispersion (Jespersen et al., 2007; Zhang et al., 2012), which could potentially extend these findings and provide additional insights into the regional cortical gray matter microstructure. Our data indicate the specificity of diffusion-driven contrasts to distinct layers across the cortical gray matter, as evidenced from the observed consistency in the cortical depth dependence of diffusion properties for studied regions (Brodmann areas 9, 4, 3b, 17) across three subjects. Understanding the variability in area-specific diffusion contrasts as well as characterizing their sensitivity to the intrinsic inter-subject variation in cortical microstructure across human brains, however, warrants further work. Quantitative variation in FA across cortical depth in our study was examined along linear profiles and was limited to relatively small regions of the studied cortical areas. Future work using more sophisticated approaches, e.g., equi-volume models (Waehnert et al., 2014) for computing cortical profiles, will enable more accurate quantitative analysis of the laminar cortical structure based on the diffusion-driven contrasts. It is also necessary to note that sensitivity of fiber orientation distributions estimated from the HARDI data to the response function calibration is well-known (Parker et al., 2013), and holds for our data as well. The response function coefficients in this study were estimated from high anisotropy voxels contained in the subcortical white matter for each specimen; however, owing to the presence of fiber populations traversing the subcortical white matter region in more than one direction, voxels in this region may not truly represent the diffusion profile of a single fiber population, which could adversely affect

the robustness and angular resolution of estimated fODF peaks (Parker et al., 2013; Tax et al., 2014). Lastly, our data were acquired from cortical tissue ex vivo and thus reflect known alterations in MR properties as a result of fixation with shortened T_2-relaxation time and lower diffusivity relative to in vivo tissue (Dawe et al., 2009). While this does not influence the interpretation of orientation-based contrasts and histological comparison across cortical areas, it necessitated the use of heavier diffusion-weighting in our study with shortest achievable echo times in order to offset the exacerbation in SNR loss due to both these factors.

In conclusion, our findings demonstrate unique sensitivity of diffusion MRI to resolve the complex microstructure of cortical gray matter and differentiate its region-specific heterogeneity across human cortical areas. The results of this work have useful implications for three-dimensional myeloarchitectonic mapping of cortical areas, and will also significantly benefit the interpretation of diffusion contrasts in the human cortex in vivo. Furthermore, direct histological comparison of dMRI findings reported here will contribute to further understanding of the basis of diffusion-encoded MR contrasts in relatively complex cortical gray matter microenvironments.

Supplementary Material

Refer to Web version on PubMed Central for supplementary material.

Acknowledgments

This work was supported by the National Institutes of Health grants R03EB017806 (to M.A) and R01NS084957 (to S.M). The authors thank Dr. Olga Pletnikova for help with brain procurement for this research.

References

Aggarwal M, Gobius I, Richards LJ, Mori S. Diffusion MR Microscopy of Cortical Development in the Mouse Embryo. Cereb Cortex. 201410.1093/cercor/bhu006

Aggarwal M, Mori S, Shimogori T, Blackshaw S, Zhang J. Three-dimensional diffusion tensor microimaging for anatomical characterization of the mouse brain. Magn Reson Med. 2010; 64:249–261. [PubMed: 20577980]

Amunts K, Malikovic A, Mohlberg H, Schormann T, Zilles K. Brodmann's areas 17 and 18 brought into stereotaxic space-where and how variable? Neuroimage. 2000; 11:66–84. [PubMed: 10686118]

Amunts, K.; Schleicher, A.; Zilles, K. Architectonic mapping of the human cerebral cortex. In: Schuz, A.; Miller, R., editors. Cortical areas: unity and diversity. Taylor & Francis; New York: 2002.

Anwander, A.; Pampel, A.; Knosche, TR. In vivo measurement of cortical anisotropy by diffusion-weighted imaging correlates with cortex type. Proceedings of the International Society for Magnetic Resonance in Medicine; 2010. p. 109

Anwander A, Tittgemeyer M, von Cramon DY, Friederici AD, Knosche TR. Connectivity-Based Parcellation of Broca's Area. Cereb Cortex. 2007; 17:816–825. [PubMed: 16707738]

Augustinack JC, Magnain C, Reuter M, van der Kouwe AJ, Boas D, Fischl B. MRI parcellation of ex vivo medial temporal lobe. Neuroimage. 2014; 93(Pt 2):252–259. [PubMed: 23702414]

Baillarger J. Recherches sur la structure de la couche corticale des circonvolutions du cerveau. Mem Acad R Med. 1840; 8:149–183.

Barbier EL, Marrett S, Danek A, Vortmeyer A, van Gelderen P, Duyn J, Bandettini P, Grafman J, Koretsky AP. Imaging cortical anatomy by high-resolution MR at 3.0T: detection of the stripe of Gennari in visual area 17. Magn Reson Med. 2002; 48:735–738. [PubMed: 12353293]

Basser PJ, Mattiello J, LeBihan D. MR diffusion tensor spectroscopy and imaging. Biophys J. 1994; 66:259–267. [PubMed: 8130344]

Behrens TE, Johansen-Berg H. Relating connectional architecture to grey matter function using diffusion imaging. Philos Trans R Soc Lond B Biol Sci. 2005; 360:903–911. [PubMed: 16087435]

Behrens TE, Woolrich MW, Jenkinson M, Johansen-Berg H, Nunes RG, Clare S, Matthews PM, Brady JM, Smith SM. Characterization and propagation of uncertainty in diffusion-weighted MR imaging. Magn Reson Med. 2003; 50:1077–1088. [PubMed: 14587019]

Brodmann, K. Vergleichende Lokalisationslehre der Großhirnrinde in ihren Prinzipien dargestellt auf Grund des Zellenbaues. Leipzig: Barth; 1909. [repr: Garey, L.J. (trans., ed.) (1994) Localization in the cerebral cortex. London: Smith-Gordon]

Calamante F, Tournier JD, Jackson GD, Connelly A. Track-density imaging (TDI): super-resolution white matter imaging using whole-brain track-density mapping. Neuroimage. 2010; 53:1233–1243. [PubMed: 20643215]

Dawe RJ, Bennett DA, Schneider JA, Vasireddi SK, Arfanakis K. Postmortem MRI of human brain hemispheres: T2 relaxation times during formaldehyde fixation. Magn Reson Med. 2009; 61:810–818. [PubMed: 19189294]

Dyrby TB, Baare WF, Alexander DC, Jelsing J, Garde E, Sogaard LV. An ex vivo imaging pipeline for producing high-quality and high-resolution diffusion-weighted imaging datasets. Hum Brain Mapp. 2011; 32:544–563. [PubMed: 20945352]

Eickhoff S, Walters NB, Schleicher A, Kril J, Egan GF, Zilles K, Watson JD, Amunts K. High-resolution MRI reflects myeloarchitecture and cytoarchitecture of human cerebral cortex. Hum Brain Mapp. 2005; 24:206–215. [PubMed: 15543596]

Fischl, B. Estimating the Location of Brodmann Areas from Cortical Folding Patterns Using Histology and Ex Vivo MRI. In: Geyer, S.; Turner, R., editors. Microstructural Parcellation of the Human Cerebral Cortex. Springer; Berlin Heidelberg: 2013. p. 129-156.

Fischl B, Dale AM. Measuring the thickness of the human cerebral cortex from magnetic resonance images. Proc Natl Acad Sci U S A. 2000; 97:11050–11055. [PubMed: 10984517]

Fukunaga M, Li TQ, van Gelderen P, de Zwart JA, Shmueli K, Yao B, Lee J, Maric D, Aronova MA, Zhang G, Leapman RD, Schenck JF, Merkle H, Duyn JH. Layer-specific variation of iron content in cerebral cortex as a source of MRI contrast. Proc Natl Acad Sci U S A. 2010; 107:3834–3839. [PubMed: 20133720]

Geyer S, Weiss M, Reimann K, Lohmann G, Turner R. Microstructural Parcellation of the Human Cerebral Cortex - From Brodmann's Post-Mortem Map to in vivo Mapping with High-Field Magnetic Resonance Imaging. Front Hum Neurosci. 2011; 5:19. [PubMed: 21373360]

Haroon, HA.; Binney, RJ.; Parker, GJ. Probabilistic quantification of regional cortical microstructural complexity. Proceedings of the International Society for Magnetic Resonance in Medicine; 2010. p. 578

Heidemann RM, Porter DA, Anwander A, Feiweier T, Heberlein K, Knosche TR, Turner R. Diffusion imaging in humans at 7T using readout-segmented EPI and GRAPPA. Magn Reson Med. 2010; 64:9–14. [PubMed: 20577977]

Jaermann T, De Zanche N, Staempfli P, Pruessmann KP, Valavanis A, Boesiger P, Kollias SS. Preliminary experience with visualization of intracortical fibers by focused high-resolution diffusion tensor imaging. AJNR Am J Neuroradiol. 2008; 29:146–150. [PubMed: 17947372]

Jespersen SN, Kroenke CD, Ostergaard L, Ackerman JJ, Yablonskiy DA. Modeling dendrite density from magnetic resonance diffusion measurements. Neuroimage. 2007; 34:1473–1486. [PubMed: 17188901]

Jiang H, van Zijl PC, Kim J, Pearlson GD, Mori S. DtiStudio: resource program for diffusion tensor computation and fiber bundle tracking. Comput Methods Programs Biomed. 2006; 81:106–116. [PubMed: 16413083]

Jones DK, Horsfield MA, Simmons A. Optimal strategies for measuring diffusion in anisotropic systems by magnetic resonance imaging. Magn Reson Med. 1999; 42:515–525. [PubMed: 10467296]

Kim EY, Kim DH, Chang JH, Yoo E, Lee JW, Park HJ. Triple-layer appearance of Brodmann area 4 at thin-section double inversion-recovery MR imaging. Radiology. 2009; 250:515–522. [PubMed: 19098226]

Kleinnijenhuis M, Zerbi V, Kusters B, Slump CH, Barth M, van Cappellen van Walsum AM. Layer-specific diffusion weighted imaging in human primary visual cortex in vitro. Cortex. 2013; 49:2569–2582. [PubMed: 23347559]

Kroenke CD, Van Essen DC, Inder TE, Rees S, Bretthorst GL, Neil JJ. Microstructural changes of the baboon cerebral cortex during gestational development reflected in magnetic resonance imaging diffusion anisotropy. J Neurosci. 2007; 27:12506–12515. [PubMed: 18003829]

Leuze CW, Anwander A, Bazin PL, Dhital B, Stuber C, Reimann K, Geyer S, Turner R. Layer-specific intracortical connectivity revealed with diffusion MRI. Cereb Cortex. 2014; 24:328–339. [PubMed: 23099298]

McKinstry RC, Mathur A, Miller JH, Ozcan A, Snyder AZ, Schefft GL, Almli CR, Shiran SI, Conturo TE, Neil JJ. Radial organization of developing preterm human cerebral cortex revealed by non-invasive water diffusion anisotropy MRI. Cereb Cortex. 2002; 12:1237–1243. [PubMed: 12427675]

McNab JA, Jbabdi S, Deoni SC, Douaud G, Behrens TE, Miller KL. High resolution diffusion-weighted imaging in fixed human brain using diffusion-weighted steady state free precession. Neuroimage. 2009; 46:775–785. [PubMed: 19344686]

McNab JA, Polimeni JR, Wang R, Augustinack JC, Fujimoto K, Stevens A, Triantafyllou C, Janssens T, Farivar R, Folkerth RD, Vanduffel W, Wald LL. Surface based analysis of diffusion orientation for identifying architectonic domains in the in vivo human cortex. Neuroimage. 2013; 69:87–100. [PubMed: 23247190]

Miller KL, Stagg CJ, Douaud G, Jbabdi S, Smith SM, Behrens TE, Jenkinson M, Chance SA, Esiri MM, Voets NL, Jenkinson N, Aziz TZ, Turner MR, Johansen-Berg H, McNab JA. Diffusion imaging of whole, post-mortem human brains on a clinical MRI scanner. Neuroimage. 2011; 57:167–181. [PubMed: 21473920]

Mori S, van Zijl PC. A motion correction scheme by twin-echo navigation for diffusion-weighted magnetic resonance imaging with multiple RF echo acquisition. Magn Reson Med. 1998; 40:511–516. [PubMed: 9771567]

Nagy Z, Alexander DC, Thomas DL, Weiskopf N, Sereno MI. Using high angular resolution diffusion imaging data to discriminate cortical regions. PLoS One. 2013; 8:e63842. [PubMed: 23691102]

Nieuwenhuys R. The myeloarchitectonic studies on the human cerebral cortex of the Vogt-Vogt school, and their significance for the interpretation of functional neuroimaging data. Brain Struct Funct. 2013; 218:303–352. [PubMed: 23076375]

Parker GD, Marshall D, Rosin PL, Drage N, Richmond S, Jones DK. A pitfall in the reconstruction of fibre ODFs using spherical deconvolution of diffusion MRI data. Neuroimage. 2013; 65:433–448. [PubMed: 23085109]

Preuss TM, Coleman GQ. Human-specific organization of primary visual cortex: alternating compartments of dense Cat-301 and calbindin immunoreactivity in layer 4A. Cereb Cortex. 2002; 12:671–691. [PubMed: 12050080]

Reese TG, Heid O, Weisskoff RM, Wedeen VJ. Reduction of eddy-current-induced distortion in diffusion MRI using a twice-refocused spin echo. Magn Reson Med. 2003; 49:177–182. [PubMed: 12509835]

Tax CM, Jeurissen B, Vos SB, Viergever MA, Leemans A. Recursive calibration of the fiber response function for spherical deconvolution of diffusion MRI data. Neuroimage. 2014; 86:67–80. [PubMed: 23927905]

Tournier JD, Calamante F, Connelly A. Robust determination of the fibre orientation distribution in diffusion MRI: non-negativity constrained super-resolved spherical deconvolution. Neuroimage. 2007; 35:1459–1472. [PubMed: 17379540]

Tournier JD, Calamante F, Connelly A. MRtrix: Diffusion tractography in crossing fiber regions. International Journal of Imaging Systems and Technology. 2012; 22:53–66.

Truong TK, Guidon A, Song AW. Cortical depth dependence of the diffusion anisotropy in the human cortical gray matter in vivo. PLoS One. 2014; 9:e91424. [PubMed: 24608869]

Tuch DS, Reese TG, Wiegell MR, Makris N, Belliveau JW, Wedeen VJ. High angular resolution diffusion imaging reveals intravoxel white matter fiber heterogeneity. Magn Reson Med. 2002; 48:577–582. [PubMed: 12353272]

Vogt C, Vogt O. Allgemeinere Ergebnisse unserer Hirnforschung. J Psychol Neurol. 1919; 25:292–398.

Waehnert MD, Dinse J, Weiss M, Streicher MN, Waehnert P, Geyer S, Turner R, Bazin PL. Anatomically motivated modeling of cortical laminae. Neuroimage. 2014; 93(Pt 2):210–220. [PubMed: 23603284]

Wedeen VJ, Hagmann P, Tseng WY, Reese TG, Weisskoff RM. Mapping complex tissue architecture with diffusion spectrum magnetic resonance imaging. Magn Reson Med. 2005; 54:1377–1386. [PubMed: 16247738]

White LE, Andrews TJ, Hulette C, Richards A, Groelle M, Paydarfar J, Purves D. Structure of the human sensorimotor system. I: Morphology and cytoarchitecture of the central sulcus. Cereb Cortex. 1997; 7:18–30. [PubMed: 9023429]

Yamamoto T, Hirano A. A comparative study of modified Bielschowsky, Bodian and thioflavin S stains on Alzheimer's neurofibrillary tangles. Neuropathol Appl Neurobiol. 1986; 12:3–9. [PubMed: 2422580]

Zhang H, Schneider T, Wheeler-Kingshott CA, Alexander DC. NODDI: practical in vivo neurite orientation dispersion and density imaging of the human brain. Neuroimage. 2012; 61:1000–1016. [PubMed: 22484410]

Zilles, K.; Amunts, K. Architecture of the cerebral cortex. In: Mai, JK.; Paxinos, G., editors. The Human Nervous System. Academic Press; San Diego: 2012. p. 836-895.

Highlights

- High angular- and spatial-resolution 3D diffusion MRI of human cortical areas
- Region-specific dMRI contrasts evident in Brodmann areas 9, 4, 3b, and 17
- dMRI results compared with silver impregnation to elucidate microstructural basis
- Findings show dMRI is sensitive to laminar heterogeneity of human cortical myeloarchitecture

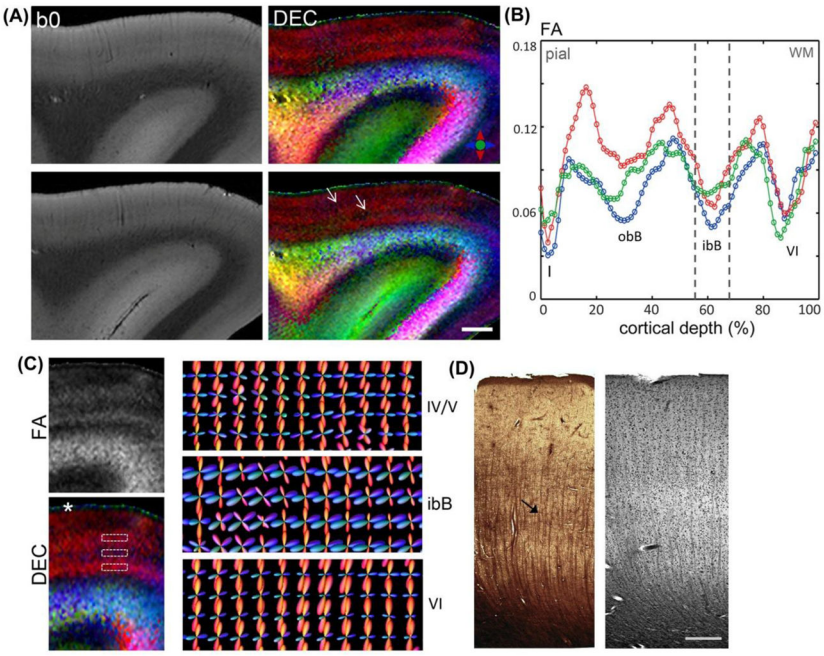

Figure 1.

Diffusion microimaging of cortical gray matter in the prefrontal cortex (Brodmann area 9). **A)** b0 images and corresponding DEC maps of two slices through the superior frontal gyrus. White arrows indicate two zones of low anisotropy compared to adjacent layers resolved parallel to the cortical surface. **B)** FA profiles measured across cortical depth in the three subjects (denoted by red, blue, green). Values plotted are the mean FA measurements averaged over cortical depth profiles within regions of 4-mm thickness in each subject. Dashed lines indicate the position of the local minimum corresponding to the inner band of Baillarger (ibB); obB: outer band of Baillarger, Roman numerals denote cortical layers. **C)** Left, Magnified views of FA and DEC maps across cortical gray matter. White asterisk marks cortical layer I, demarcated by a sharp transition from the radially-oriented anisotropy of underlying layers. Right, Reconstructed fODFs in cortical laminae (regions marked by dashed white boxes in the DEC map) indicate prominent radial and tangential peaks resolved in the ibB compared to adjacent layers. **D)** Silver-impregnated section through area 9 (left) and luxol fast blue section co-stained with H&E for marking cell nuclei (right). Black arrow indicates faintly-stained dense horizontal fibers evident in the ibB in the silver-stained section. Scale bar for A = 2 mm, scale bar for D = 0.5 mm.

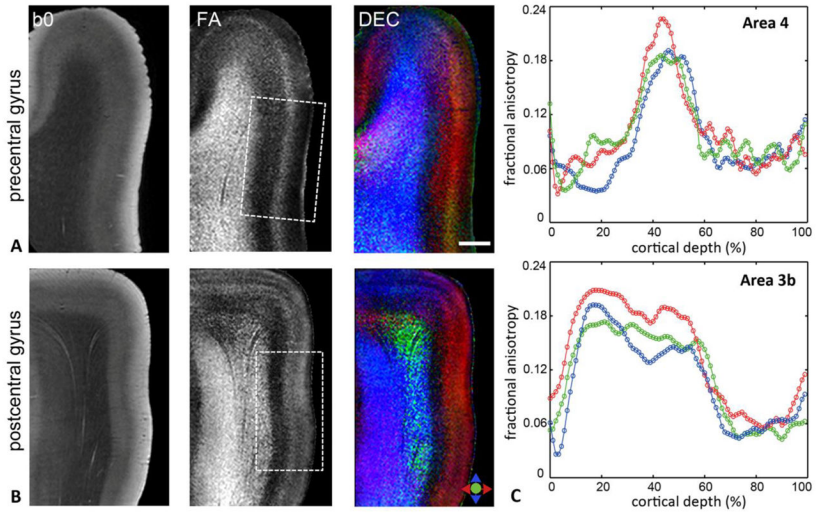

Figure 2.

A–B) b0, FA, and DEC maps through the precentral and postcentral gyri demonstrate region-specific contrasts resolved in the primary motor (area 4) and primary somatosensory (area 3b) cortices (areas indicated by the dashed white boxes). Colors in the DEC maps denote the primary orientation of diffusion as indicated by the color index. **C)** Plots show quantitative FA profiles measured as a function of cortical depth from the pial surface in areas 4 (top) and 3b (bottom) for the three subjects. Values plotted are mean FA measurements calculated over regions-of-interest of ~4 mm thickness in the cortical gray matter, with the abscissa normalized to percentage of total cortical depth for each subject. Scale bar = 2 mm.

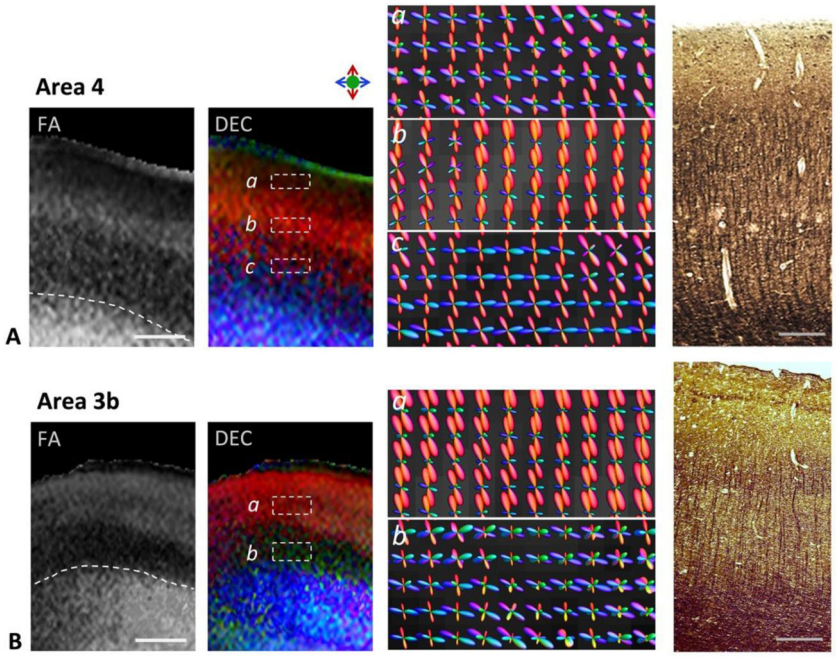

Figure 3.

Region-specific differences in the M1 (area 4, top panel) and S1 (area 3b, bottom panel) cortical areas seen with diffusion contrasts and estimated fiber orientation distributions across cortical depth. Representative sections through areas 4 and 3b with FA and DEC contrasts are shown. Dashed white lines indicate the boundary between gray matter and subcortical white matter in the FA maps. Panels *a–c* (in A) and *a–b* (in B) are high-magnification views showing reconstructed fODFs in different regions across the cortical depth (areas marked by dashed white boxes in DEC maps) in areas 4 and 3b, respectively. fODF surfaces are colored based on 3D spatial orientation as indicated by the color index. Corresponding silver-impregnated histological sections from areas 4 and 3b are shown in the right panel. Scale bars = 1 mm, scale bars for histology sections = 0.5 mm.

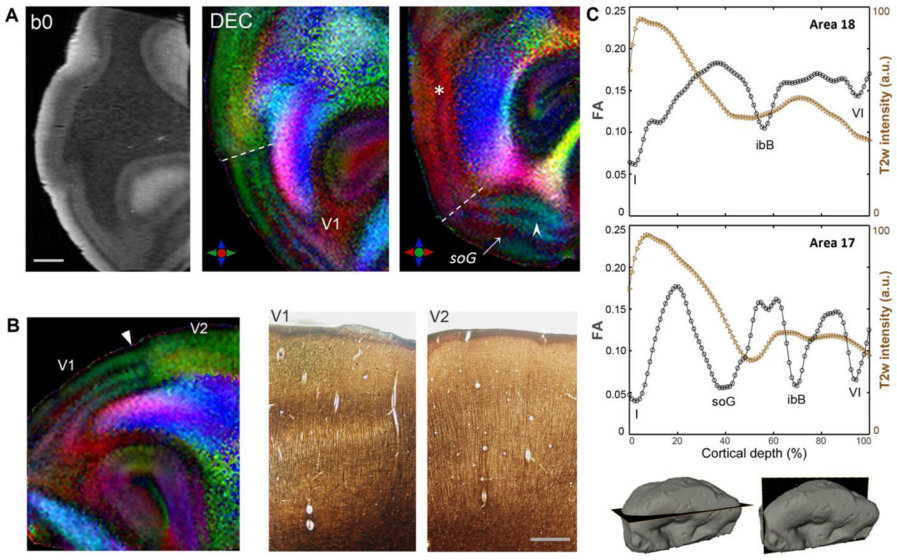

Figure 4.

Laminar structure of the human visual cortex (Brodmann areas 17, 18) delineated with diffusion MRI. **A)** b0 image and corresponding DEC contrasts in orthogonal planes through the occipital lobe. The anatomical locations of the sections are indicated in the surface reconstructions at the bottom right. Two distinct layers marked by tangential diffusion anisotropy can be resolved in the primary visual area (V1), corresponding to the stria of Gennari in layer IV (soG, white arrow) and the ibB in layer V (white arrowhead). A marked transition in laminar structure between V1 and the secondary visual area V2 is clearly delineated (dashed white lines). Asterisk marks the tangential ibB resolved in V2. **B)** Magnified view of DEC map demonstrates the transition in diffusion MR contrasts resolved at the V1/V2 border (white arrowhead, left), which closely mirrors the change in layered architecture seen with silver-stained sections adjacent to the V1-V2 boundary (right). **C)** FA and T_2w intensity profiles across areas 18 (top) and 17 (bottom) plotted as a function of cortical depth. Local minima in FA profiles correspond to bands of tangential fibers in distinct cortical layers indicated by Roman numerals. Scale bar in A = 2 mm, scale bar in B = 0.5 mm.

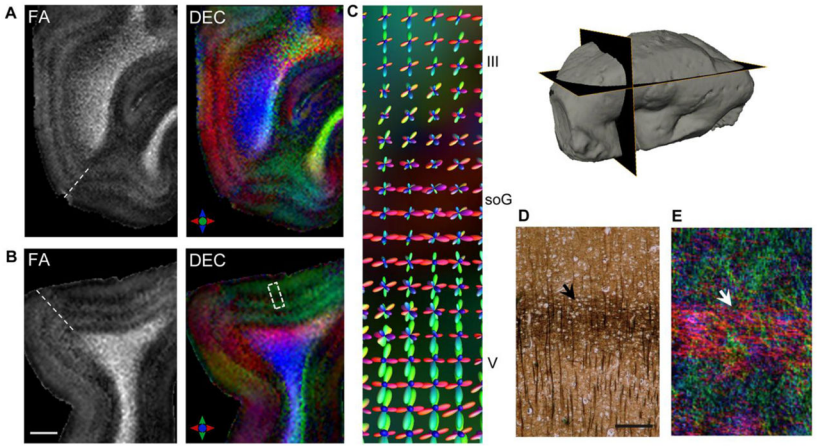

Figure 5.

Delineation of the stria of Gennari (soG) based on diffusion MR contrasts in the primary visual area (Brodmann area 17). **A–B)** FA and DEC maps in orthogonal views demonstrate layer-specific variation in anisotropy resolved across the cortical gray matter. Note that the plane of the sections in A–B intersects the V1 surface at an oblique angle owing to the curvature of the cortical surface (indicated in the surface reconstruction at the top right). **C)** Magnified view shows reconstructed fODFs overlaid on the DEC map (corresponding to a small region within the dashed white box in B), indicating dominant tangential peaks in the soG in comparison to inner and outer adjoining cortical layers. Silver-impregnated histological section at the level of the soG **(D)** demonstrates the horizontal plexus of densely labeled fibers in the soG (black arrow) with radially-oriented fibers apparent in adjacent layers. **E)** Track-density map generated from probabilistic tractography indicates a band of dense crossing horizontal fibers corresponding to the soG (white arrow) and intervening radial fiber orientations resolved with the HARDI data. Scale bar for A-B = 2 mm, scale bar in D = 250 μm.

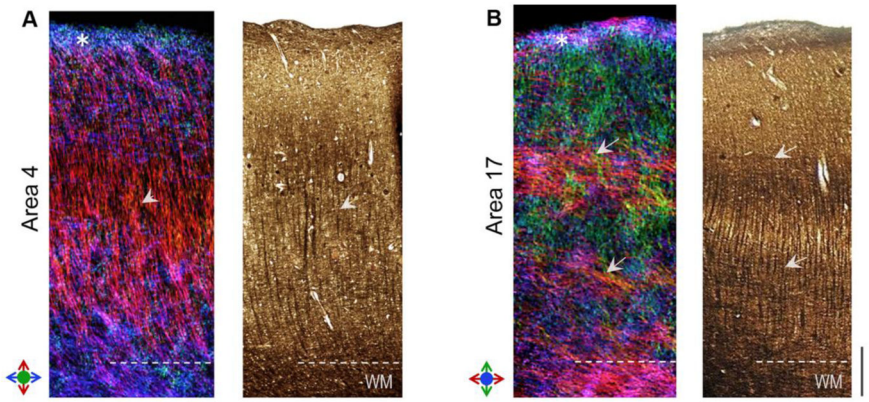

Figure 6.

Comparison of region-specific microstructure of the astriate (primary motor, area 4) and bistriate (primary visual, area 17) cortical areas resolved with dMRI. Track-density maps of area 4 (left panel) and area 17 (right panel) are compared with Bielschowsky silver impregnation of the two areas. Colors in TDI maps denote the local orientation of fibers as indicated by the color indexes. Arrowheads in A indicate a high density of radial fibers resolved in the mid-cortical layers of area 4. Arrows in B mark the distinct bands of tangential fibers resolved in area 17, corresponding to the inner and outer bands of Baillarger. White asterisks mark cortical layer I delineated in dMRI contrasts in both A and B. Scale bar = 0.5 mm.